Article

pubs.acs.org/Biomac

Photoinduced Development of Antibacterial Materials Derived from Isosorbide Moiety

Cedric Lorenzini,[†] Adnan Haider,[‡] Inn-Kyu Kang,[‡] Marco Sangermano,[§] Samir Abbad-Andalloussi,[∥] Pierre-Emmanuel Mazeran,[⊥] Jacques Lalevée,[#] Estelle Renard,[†] Valérie Langlois,[†] and Davy-Louis Versace*[,†]

[†]Institut de Chimie et des Matériaux Paris-Est, Equipe Systèmes Polymères Complexes, UMR 7182, CNRS-Université Paris-Est Créteil (UPEC) 2-8 rue Henri Dunant, 94320 Thiais, France

[‡]Department of Polymer Science and Engineering, Kyungpook National University, Daegu 702-701, South Korea

[§]Politecnico di Torino, Dipartimento di Scienza Applicata e Tecnologia, C.so Duca degli Abruzzi 24, 10129 Torino, Italy

[∥]Unité Bioemco Equipe IBIOS, UMR 7618 CNRS - Université Paris-Est Créteil Val-de-Marne, 61, Avenue Général de Gaulle, Créteil 94010 CEDEX, France

[⊥] Laboratoire Roberval, UMR CRNS-UTC 7337, Centre de Recherche de Royallieu, Université de Technologie de Compiègne, Compiègne 60205 CEDEX, France

[#]Institut de Science des Matériaux de Mulhouse, IS2M-LRC 7228, 15 rue Jean Starcky, 68057 Mulhouse, France

Supporting Information

ABSTRACT: A straightforward method for immobilizing in situ generated silver nanoparticles on the surface of a photoactivable isosorbide-derived monomer is developed with the objective to design a functional material having antibacterial properties. The photoinduced thiol−ene mechanism involved in these syntheses is described by the electron spin resonance/spin trapping technique. The resulting materials with or without silver nanoparticles (Ag NPs) were used as films or as coatings on glass substrate. The surface of the synthesized materials was characterized by X-ray photoelectron spectroscopy and scanning electron microscopy, and their thermal and mechanical properties were evaluated by dynamic-mechanical thermal tests, differential scanning calorimetry, thermogravimetric analyses, along with pencil hardness, nanoindentation, and scratch resistance tests. The photoinduced formation of Ag NPs is also confirmed by UV spectrophotometry. Finally, a primary investigation demonstrates the antibacterial properties of the isosorbide-derived material against *Staphylococcus aureus* and *Escherichia coli*, as well as its cytocompatibility toward NIH 3T3 fibroblastic cells.

INTRODUCTION

Infections by pathogens generally resulting from the adhesion/proliferation of bacteria on medical devices remain a major concern. It was estimated that 100 000 deaths occurred among the 1.7 million hospital-acquired infections in 2002 in the United States. In response to this threat, three main approaches have been investigated to prevent the bacterial colonization of materials: the first one is based on lethal contact which induces the biochemical death of bacteria,[1] a second alternative consists of immobilizing photosentitizers,[2−5] and the final approach concerns biocide leaching.[6−14]

Among the metal nanoparticles used in the biocide leaching process, silver nanoparticles (Ag NPs) have demonstrated to be the most efficient antimicrobial agents toward pathogenic microorganisms.[15] Significant clinical cytotoxicity investigations on Ag NPs have been reported,[16] and numerous silver nanoproducts available in biomedical applications[17−19] and introduced into different food contact materials[20] have been developed; it is therefore that Ag NPs stay the most prevalent nanomaterial in more than 1000 daily life consumer products according to the Nanotechnology-based Consumer Products Inventory. Different strategies are reported in literature for the preparation of hybrid polymeric materials containing silver nanoparticles.[21−31] Among them, the photochemical process appears more beneficial than the other ones due to its many advantages[32,33] (low temperature conditions, low energy consumption, for example). The procedure typically consists of the reduction of metal salt by radicals under light activation along with the polymer network formation at the same time.[34−38] Following this approach, the preparation of hybrid coatings derived from renewable resources and containing Ag

Received: July 30, 2014
Revised: January 28, 2015

DOI: 10.1021/bm501755r
Biomacromolecules XXXX, XXX, XXX−XXX

Scheme 1. Investigated Compounds

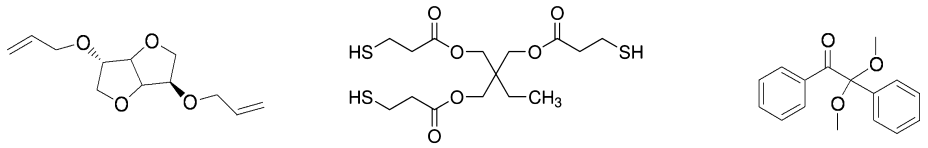

NPs generated in situ in a thiol−ene photocurable system is proposed.

The rise of interest toward monomers derived from renewable resources[39−41] leads to the creation of a multitude of materials which can find applications in the biomedical field, because of their biocompatibility and biodegradability. Among the studied sugar-based monomers, isosorbide, an 1,4:3,6-dianhydrohexitol derived from glucose, appears as one of the most interesting[42,43] due to its rigidity, chirality, and non-toxicity. Isosorbide has been mainly used to synthesize polycondensates[44−46] and to enhance thermal and mechanical properties[47−52] of materials with the aim of replacing bisphenol A. To the best of our knowledge, the synthesis of an isosorbide-derived monomer/silver hybrid material has not been examined yet. The aim of the present work is to develop films or coatings (incorporating isosorbide units) which have efficient anti-adherent and antibacterial properties against *Staphylococcus aureus* and *Escherichia coli*, and remain cytocompatible toward fibroblast cells.

The first part of this study demonstrates the ability of an isosorbide-derived monomer to be involved in the thiol−ene process through an electron spin resonance/spin trapping analysis. In a second part, a particular effort is made to demonstrate the reactivity of the isosorbide-derived monomer/trithiol/silver salt system upon light activation by real-time Fourier transform infrared spectroscopy. The in situ generation of Ag NPs in solution and within the polymer matrix upon irradiation was also demonstrated, respectively, by UV−vis spectrophotometry, scanning electron microscopy, and XPS measurements. The thermal and mechanical properties of the hybrid materials are evaluated by dynamic-mechanical thermal analyses, differential scanning calorimetry, and thermogravimetric experiments. To demonstrate the ability of the isosorbide-derived materials for being used as a coating, further mechanical investigations have been done, that is, pencil hardness, nanoindentation, and scratch resistance tests. Finally, the antibacterial property against *S. aureus* and *E. coli* and the cytocompatibility with NIH 3T3 fibroblastic cells of the silver-containing films derived from isosorbide are finally evaluated.

EXPERIMENTAL SECTION

Materials. The main compounds investigated in this study are presented in Scheme 1 and used with the best purity available. Trimethylolpropane tris(3-mercaptopropionate) (Trithiol), silver hexafluoroantimonate ($AgSbF_6$), allyl bromide, and tetrabutylammonium bromide were purchased from Aldrich. 2,2-Dimethoxy-1,2-diphenylethan-1-one (DMPA) was kindly provided by BASF company.

NIH 3T3 fibroblastic cell line was purchased from the Korea cell bank (Seoul, South Korea). Dulbecco's modified Eagle's medium (DMEM), fetal bovine serum (FBS), penicillin G-streptomycin, and phosphate buffer saline (PBS) were purchased from Gibco, Tokyo, Japan. Live/dead assay kit was purchased from Biovision, and 3-(4,5-dimethylazol-2-yl)-2,5-diphenyl-2*H*-tetrazolium bromide (MTT) assay kit was purchased from Sigma-Aldrich. All reagents and chemicals in this study were used without any further purification.

Synthesis of Diallyl Isosorbide Ether (DIALI). DIALI (I) was prepared by Williamson reaction.[30] Isosorbide (3 g, 20.4 mmol) was dissolved in a 50% aqueous NaOH (6 g, n = 107.2 mmol) solution. Allyl bromide (10 mL, n = 115.7 mmol) was used as an alkylating agent in the presence of 4.5% of tetrabutylammonium bromide (TBAB, 300 mg, n = 0.94 mmol) with respect to isosorbide. The reaction was stopped after 4 h of heating at 65 °C, and the mixture was extracted with methylene chloride. The organic phase was first washed with HCl 1 M and then with water in order to remove salts. The final product was purified by distillation (108 °C/1 Torr) with a yield of 88%. ^{1}H and ^{13}C NMR spectra of DIALI in $CDCl_3$ are displayed in Figure S1 (Supporting Information).

Synthesis of the Isosorbide-Derived Films. DIALI (M = 224 g/mol, 300 mg, n = 1.34 mmol, liquid), trithiol (M = 396 g/mol, 355 mg, n = 0.896 mmol, liquid), and DMPA (M = 256.30 g/mol, 6.5 mg, 0.025 mmol, solid) were mixed together until the complete solubilization of DMPA into the organic compounds. The later solution was then introduced in a silicon mold (4 cm × 2 cm) and irradiated with a Hg−Xe lamp from Hamamatsu (200 W, Lightning-cure LC8 (L8251)) coupled with a flexible light guide. The end of the guide was placed at a distance of 11 cm, and the maximum UV light intensity at the sample position was evaluated to be I_0 = 200 mW/cm^2. In order to avoid the oxygen diffusion through the solution and its inhibition, a polypropylene film was layered on the top of the solution upon irradiation.

For DIALI-derived films with Ag NPs, the procedure was similar as the one described previously. DIALI (M = 224 g/mol, 300 mg, n = 1.34 mmol, liquid), trithiol (M = 396 g/mol, 355 mg, n = 0.896 mmol, liquid), and DMPA (M = 256.30 g/mol, 6.5 mg, 0.025 mmol, solid) were mixed together until the complete solubilization of DMPA into the organic compounds. At the same time, silver hexafluoroantimonate ($AgSbF_6$, M = 343.62 g/mol, 13 mg, n = 0.038 mmol) was dissolved in 0.1 mL of CH_2Cl_2. Then, both solutions were gathered together, introduced in a silicon mold (4 cm × 2 cm), and irradiated according to the same procedure described in the previous paragraph. The thickness of the synthesized films (with and without Ag NPs) was 1 mm. The length and the width of the resulting films are 4 and 2 cm, respectively. The optical images of the isosorbide-derived films (with and without Ag NPs) are displayed in Figure S2 (Supporting Information).

Synthesis of the Isosorbide-Derived Coatings. The previous solutions containing Ag NPs or without Ag NPs were, respectively, applied on a glass substrate by means of a 200 μm calibrated wire-wound applicator. (The glass substrates were previously intensively rinsed with ethanol and toluene and dried under vacuum at 40 °C for one night.) A polypropylene film was laid on the top of the photosensitive layer to prevent oxygen diffusion and the coatings were irradiated according to the same procedure than the one used for the synthesis of isosorbide-derived films. The optical images of the DIALI-derived coatings with and without Ag NPs are displayed in Figure S3 (Supporting Information).

Real-Time Fourier Transform Infrared Spectroscopy. Kinetics of photopolymerization were followed by real-time Fourier transform infrared spectroscopy (RT-FTIR) using a Thermo-Nicolet 6700 instrument. The liquid samples were deposited on a BaF_2 chips by means of calibrated wire-wound applicator. The thickness of the UV-curable film was evaluated at 4 μm. The RT-FTIR analyses were carried out under laminated conditions: a polypropylene film was laid

DOI: 10.1021/bm501755r
Biomacromolecules XXXX, XXX, XXX−XXX

on the top of the photosensitive layer to prevent oxygen diffusion. Samples were irradiated during 200 s at room temperature, by means of a Lightningcure LC8 (L8251) from Hamamatsu, equipped with a Hg−Xe lamp (200 W) coupled with a flexible light guide. The end of the guide was placed at a distance of 11 cm. The maximum UV light intensity at the sample position was evaluated to be 200 mW/cm^2. The photopolymerization was monitored by the disappearance of the allyl carbon bonds of the DIALI monomer at 1647 cm^{-1} and the thiol function at 2560 cm^{-1}.

X-ray Photoelectron Spectroscopy (XPS). XPS measurements, at a mean takeoff angle of 20°, were performed with a Mac2RIBER with a resolution of 1 eV. Survey scans were done using a monochromatic Mg Kα X-ray source (12 keV, 2 mA) with a spot diameter of 25 mm^2 operated in a low power mode (24 W). A pass energy of 10 eV was used for the detailed XPS scans. XPS spectra were obtained with an energy step of 0.05 eV with a dwell time of 200 ms. The binding energy scale was fixed by assigning a binding energy of 285.1 eV to the −CH− carbon (1s) peak.

Electron Spin Resonance/Spin-Trapping (ESR-ST). ESR-ST experiments were carried out at room temperature using an X-Band spectrometer (MS 200 from Magnettech-Berlin, Berlin, Germany) (293 K) coupled with a polychromatic light irradiation (Xe−Hg lamp; Hamamatsu, L8252, 150 W). The photoregenerated radicals were trapped by phenyl-*N*-tertbutylnitrone (PBN) at room temperature. The ESR spectra simulations were generated using the PEST WINSIM program. All of the samples were prepared in a 6 mm quartz cylindrical tube and dissolved in *tert*-butylbenzene as an inert solvent.

UV−Vis Spectroscopy. UV−vis spectra were recorded on a Varian spectrophotometer (Cary 50 bio) in the range 250−800 nm. All the solutions were degassed with argon for 5 min before use.

Scanning Electron Microscopy (SEM). The morphological appearance of the films was investigated using a LEO 1530 scanning electron microscope with accelerating voltage 1 kV for InLens detector and 5 kV for Secondary Electron detector. Prior to analyses, the samples were coated with a 4 nm layer of palladium/platinium alloy in a Cressington 208 HR sputter-coater.

Mechanical Tests for the Synthesized Films. The mechanical properties of the isosorbide-derived films with and without Ag NPs were studied out using an Instron 5965 universal testing machine at a crosshead displacement rate of 2 mm/min at room temperature (23 °C). The films were cut into dumbbell shape in order to investigate tensile strength and elongation at break. The optical images of the DIALI-derived films with and without Ag NPs are displayed in Figure S4 (Supporting Information).

Differential Scanning Calorimetry (DSC) Measurements. Amounts of 6−8 mg of the isosorbide-derived films were introduced into aluminum pans and was analyzed using a PerkinElmer Diamond DSC instrument under nitrogen atmosphere. The samples were first scanned from 50 to 170 °C with a heating rate of 20 °C/min, then cooled to 70 °C at 200 °C/min, and finally heated again to 170 °C with a heating rate of 20 °C/min. The second heating run was considered for determining the glass transition temperature (T_g).

Thermogravimetric Analyses (TGA). A total of 10 mg of the isosorbide-derived films was introduced into aluminum pans and was analyzed using on a Setaram Setsys Evolution 16 thermobalance by heating the samples at a rate of 15 °C/min from 0 to 800 °C under argon atmosphere.

Pencil Hardness. The measurement of pencil hardness goes from the lowest to the highest pencil in order to determine the maximum hardness for scratching the surface of the isosorbide-derived coatings (Method: ASTMD3363-74, 2000) (Figure S3, Supporting Information). The hardness of the coating was determined relative to a standard set of pencil leads. The surface hardness is determined by scratching the leads across the coating at a controlled angle of 45°. The pencil hardness was measured using a No. 553 pencil hardness tester (Yasuda Seiki Seisakusho Ltd.). Pencils were supplied by Staedtler Mars Lumograph 100 (Germany).

Nanoindentation and Scratch Resistance Tests. Nanoindentation and scratch tests were carried out on the isosorbide-derived coatings (deposited on glass substrates, Figure S3, Supporting Information) with a Nano Indenter (Agilent Technologies G200) using a Berkovich tip (Micro Star Technologies). Twelve nanoindentation experiments per sample were performed. Samples were loaded and unloaded at constant strain rate (0.05 s^{-1}) using the continuous stiffness measurement method until an indentation depth of 10 μm. The unloading stage was performed after a hold load plateau of 300 s in order to exhibit the viscous behavior. Three scratch tests were performed; face forward, with an increasing load from 0.1 to 200 mN for a scratching distance of 500 μm.

Antiadherence Property. Initial adhesion assays were performed using two strains of bacteria (*S. aureus* and *E. coli*), namely, *S. aureus* ATCC6538 and *E. coli* ATCC25922 on the isosorbide-derived films. Prior to in vitro antibacterial tests, the bacterial strains were grown aerobically overnight in Luria−Bertani broth at 37 °C under stirring. Overnight cultures of *S. aureus* and *E. coli* grown in Luria−Bertani (LB) broth were diluted to an optical density (OD 600) of 0.05 in sterile LB broth. At this point, the samples (DIALI/Trithiol/DMPA and the DIALI/Trithiol/DMPA/$AgSbF_6$ films, 1.5 cm × 1.5 cm × 1 mm) were immersed in the culture; the corresponding vials were placed on a slantwise rotating wheel to avoid sedimentation of bacteria, incubated for 1 or 6 h at 37 °C, and shaken at 150 rpm to allow initial adhesion to occur (INFORS AG-CH 4103, Bottmingen-Basel, Switzerland). After initial adhesion (1h and 6h), the samples were rinsed seven times with sterile saline solution (NaCl, 0.9% w/v) to remove any nonadherent cells.

Colonized native and treated isosorbide films were then transferred to 2 mL of sterile saline (solution A) and vortexed for 30 s. The samples were then transferred to 2 mL of sterile saline (solution B) and sonicated in a Branson 2200 sonicator for 3 min. Samples were transferred once more to 2 mL of sterile saline (solution C) and vortexed for 30 s. The three suspensions which represent the detached biofilm population were pooled, serially diluted, and deposited on PCA medium for viable counting. A 100 μL volume of the detached viable bacteria solution was introduced onto the surface of a Plat Count agar plate. The process was repeated through a succession of 24 predried plates. Finally, the total bacterial adhesion was determined by a counting of the colony forming units (CFUs), after overnight statically incubation of the agar plates at 37 °C. Each experiment was done on 10 different isosorbide-derived films with and without Ag NPs. Levels of adhesion were given as numbers of cells per square centimeter.

Statistical Analysis. All values corresponding to the antiadherence properties of *S. aureus* and *E. coli* are expressed as mean ± standard deviation. Statistical analysis was performed using Student's *t* test for the calculation of significance level of the data. Differences were considered statistically significant at $P < 0.05$. Ten samples per group were evaluated.

Cell Adhesion. In order to examine the interactions of the DIALI/Trithiol/DMPA and DIALI/Trithiol/DMPA/$AgSbF_6$ films with NIH 3T3 fibroblasts, cell adhesion experiments were performed according to the method previously reported.[53] Pristine isosorbide-derived films without Ag NPs (DIALI/Trithiol/DMPA) were used as a control. Briefly, circular samples (Figure S5, Supporting Information) were fitted in a 4 well culture dish and subsequently immersed in a Dulbecco's modified Eagle's medium (DMEM) containing 10% fetal bovine serum (FBS) (Gibco, Japan) and 1% penicillin G-streptomycin (Gibco, Japan). To the samples, 1 mL of the NIH 3T3 fibroblastic cells solution (3 × 10^4 cells/cm^2) were seeded on the sample and incubated in a humidified atmosphere (5% CO_2 and at 37 °C) for 1 and 3 days to determine the cell adhesion on the DIALI/Trithiol/DMPA and DIALI/Trithiol/DMPA/$AgSbF_6$ films. After incubation, the supernatant was removed, washed twice with phosphate buffered saline (PBS; Gibco), and fixed with an aqueous 2.5% glutardialdehyde solution for 20 min. The sample sheet was then dehydrated and dried in a critical point drier. The surface morphology of the samples was then observed via FE-SEM (400 Hitachi; Tokyo, Japan).

Cell Proliferation. A [3-(4,5-dimethylazol-2-yl)-2,5-diphenyl-2*H*-tetrazolium bromide] (MTT) assay (Sigma-Aldrich) was used to determine the proliferation of NIH 3T3 fibroblastic cells on the DIALI/Trithiol/DMPA which are used as the control sample and on

DOI: 10.1021/bm501755r
Biomacromolecules XXXX, XXX, XXX−XXX

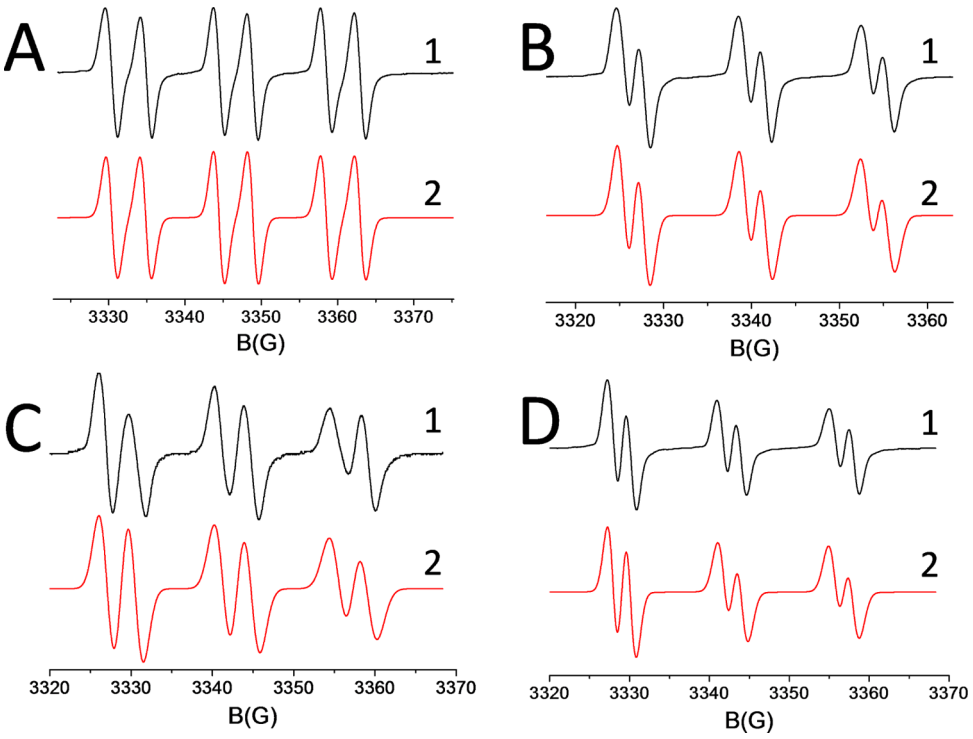

Figure 1. ESR/spin trapping with PBN of (A) DMPA, (B) DMPA/Trithiol, (C) DMPA/DIALI, and (D) DMPA/Trithiol/DIALI. Solvent = *tert*-butylbenzene. 1 = experimental spectrum, and 2 = simulated spectrum. Lamp = Hg–Xe. PBN = 0.05 M.

DIALI/Trithiol/DMPA/$AgSbF_6$ films. Briefly, NIH 3T3 fibroblastic cells were seeded at a concentration of 3×10^4 cells/mL on the DIALI/Trithiol/DMPA and DIALI/Trithiol/DMPA/$AgSbF_6$ materials, which were fitted in a 24-well plate, and cell proliferation was monitored after 1 and 3 days incubation. A 3-(4,5-dimethylazol-2-yl)-2,5-diphenyl-2*H*-tetrazolium bromide assay[54] (MTT) (Gibco) solution (50 μL, 5 mg/mL in PBS) was added to each well and incubated in a humidified atmosphere containing 5% CO_2 at 37 °C for 4 h. After removing the medium, the converted dye was dissolved in acidic isopropanol (0.04 N HCl-isopropanol) and kept in the dark at room temperature for 30 min. From each sample, the medium (100 μL) was taken, transferred to a 96-well plate, and subjected to ultraviolet measurements for the converted dye at a wavelength of 570 nm on a kinetic microplate reader (EL x 800, Bio-T Instruments, Inc., Highland Park). Each experiment was done on six different isosorbide-derived films with and without Ag NPs.

Cell Viability. A standard live/dead assay was used to evaluate cell viability after culturing NIH 3T3 fibroblast cells on DIALI/Trithiol/DMPA and DIALI/Trithiol/DMPA/$AgSbF_6$ films for 3 days based on the previously reported method.[55] Briefly the fibroblast cells were suspended in PBS with a cell density of 1×10^5–1×10^6 cells/mL. Subsequently, 200 μL of a cell suspension was mixed with 100 μL of assay solution [10 μL of calcein-AM solution (1 mM in dimethyl sulfoxide (DMSO)) and 5 μL of propidium iodide (1.5 mM in H_2O) was mixed with 5 mL of PBS] and incubated for 15 min at 37 °C. The cells were examined by fluorescence microscopy with using a band-pass filter (Nikon Eclipse E600-POL, Japan).

Silver Release Experiments. The silver release experiment was performed for the measurement of the amount of silver release from the isosorbide-derived films containing Ag NPs (Figure S5, Supporting Information). The phosphate buffer saline (PBS) was used as the medium for the silver release experiment. The amount of silver nanoparticles released from the sample was conducted by immersing the Ag containing films (circular samples with a 1.5 cm diameter, Figure S5, Supporting Information) in 10 mL of phosphate buffer saline (PBS) (pH 7.0) for different time periods (16 days). Then, the concentration of silver in phosphate buffer saline (PBS) was determined by inductively coupled plasma spectrophotometer (ICP; Thermo Jarrell Ash IRIS-AP).

RESULTS AND DISCUSSION

Reactivity of the Thiol–Ene Photoactivable System. The thiol–ene reaction has been of interest to researchers in other areas of synthesis because of its "click" characteristics. There are several features affiliated with this reaction that make it an interesting process.[56] Generally, the thiol–ene reaction has been conducted under radical conditions, often photochemically induced. However, no studies have demonstrated, for instance, the thiol–ene reactivity of a trithiol when added to DIALI monomer (under light activation) according to an ESR/spin-trapping approach. Such an investigation highlights the reactivity of the Trithiol/DIALI/DMPA system under light activation.

Figure 1 displays the different radical photoadducts which are trapped by PBN during the light activation of DMPA, DMPA/Trithiol, DMPA/DIALI, and DMPA/Trithiol/DIALI. The hyperfine coupling constant values of the corresponding radical spin adducts with PBN are summarized in Table 1. In nonaerated medium, the photolysis of DMPA (reaction r1) demonstrates the formation of benzoyl radicals[57] (aN = 14.1 G and aH = 4.4 G, Figure 1A). Upon addition of the Trithiol to DMPA, thiyl radicals are now detected (aN = 13.9 G and aH = 2.2 G, Figure 1B) and are in accordance with literature data,[58] thus underlining the H abstraction from the Trithiol by benzoyl radicals according to r2. A new carbon-centered radical (aN = 14.3 G and aH = 3.4 G, Figure 1C) is observed when using the DMPA/DIALI system, thus resulting in the free radical addition of benzoyl radicals onto allyl functions r3. When using DMPA/Trithiol/DIALI system, the direct addition of the thiyl radical across the C=C bond yields an intermediate carbon-centered radical with the concomitant generation of a

DOI: 10.1021/bm501755r
Biomacromolecules XXXX, XXX, XXX–XXX

Table 1. Hyperfine Coupling Constant Values of Radical Spin Adducts with PBN after 30 s of Irradiation of DMPA, DMPA/Trithiol, DMPA/DIALI, and DMPA/Trithiol/DIALI[a]

systems	hyperfine coupling constant values aN (G)	aH (G)	nature of the radicals trapped
DMPA	14.1	4.4	benzoyl radicals
DMPA/Trithiol	13.9	2.2	thiyl radicals
DMPA/DIALI	14.3	3.4	carbon-centered radicals
DMPA/Trithiol/DIALI	13.9	2.2	thiyl radicals

[a]Irradiation with a Hg−Xe lamp. Solution is degassed with argon for 5 min.

new thiyl radical (aN = 13.9 G and aH = 2.2 G, Figure 1D). According to these results, it is worth noticing that DMPA/Trithiol/DIALI is an efficient system for being used in a thiol−ene process.

$$\text{DMPA} \rightarrow C_6H_5C(=O)^{\bullet} + C_6H_5(OCH_3)_2C^{\bullet} \ (h\nu) \qquad \text{(r1)}$$

$$C_6H_5C(=O)^{\bullet} \ (\text{or } C_6H_5(OCH_3)_2C^{\bullet}) + \text{RSH} \rightarrow C_6H_5C(=O)H \ (\text{or } C_6H_5(OCH_3)_2CH) + \text{RS}^{\bullet}$$

$$(\text{RSH} = \text{trithiol}) \qquad \text{(r2)}$$

$$C_6H_5C(=O)^{\bullet} + R_1{-}CH{=}CH_2 \rightarrow R_1{-}C(H)^{\bullet}{-}CH_2{-}(O{=})CC_6H_5$$

$$(R_1{-}CH{=}CH_2 = \text{daillyl isosorbide}) \qquad \text{(r3)}$$

Evidence of the thiol−ene process in the DIALI/DMPA/Trithiol system has been investigated at room temperature by following the decrease of the intensity of the band associated with the thiol function (of Trithiol) and the carbon double bonds of DIALI by RT-FTIR (Figure 2). The influence of the addition of the $AgSbF_6$ salt on the thiol−ene reaction has also been described. Figure 2A and Figure 2B display respectively the disappearance of the C=C bonds (of DIALI) and the SH functions (of the Trithiol) upon light activation in the presence or not of $AgSbF_6$ salt. It is worth noticing that the final conversion of the C=C bonds (of DIALI) reaches respectively 100% and 95% after 200 s of irradiation without and with the presence of silver salt. The SH conversion is not fully completed, thus reaching, respectively, 90% and 80% without and with Ag salt. This difference could be explained as follows: a part of the benzoyl and α,α-dimethoxybenzyl radicals which are generated from the photolysis of DMPA r1 are oxidized by silver salt[59] (thus forming the α,α-dimethoxybenzyl cation) and are used neither to initiate the polymerization of DIALI nor to abstract hydrogen atom from the SH function. Due to the high affinity of silver NPs to thiol functions, it is likely that the remaining free SH group reacts with silver NPs.[60,61] The photogenerated α,α-dimethoxybenzyl cation is then complexing with the counterion SbF_6^-.

Under the same conditions of irradiation, and in the presence of 2 wt % of DMPA, a low conversion of the C=C of DIALI (28%) is noticed after 200 s of irradiation (inset in Figure 2A), thus showing that the allyl bonds of DIALI are not prone to homopolymerize. This result is in agreement with the low rate

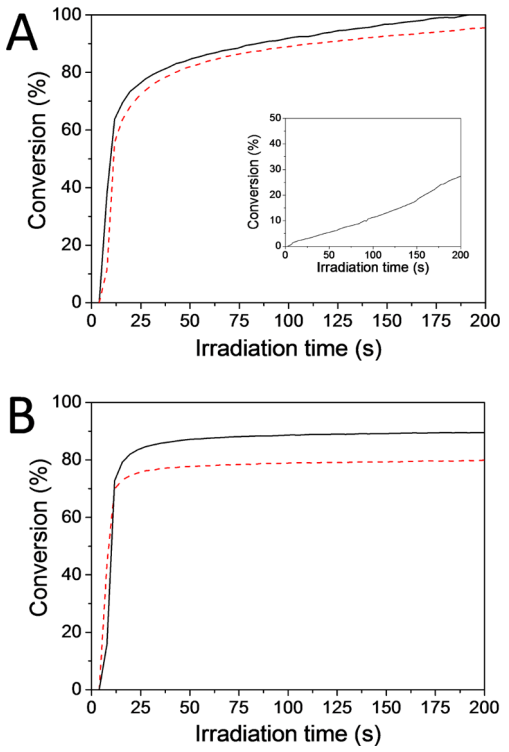

Figure 2. Thiol−ene photoaddition kinetics of the Trithiol onto DIALI with or without the presence of $AgSbF_6$. (A) Conversion of the allyl function and (B) conversion of the thiol function under light activation. Solid line = DIALI/Trithiol/DMPA system. Dotted line = DIALI/Trithiol/DMPA/$AgSbF_6$ system. Intensity = 200 mW/cm^2. Inset in (A) = Photopolymerization of DIALI with DMPA: conversion of the allyl bonds as a function of irradiation time (200 mW/cm^2).

constant of addition (7.5×10^3 M^{-1} s^{-1}) of carbon radicals on alkenes.[33,62]

Evidence of the Silver NPs Formation. Figure 3 shows the typical evolution of the absorption spectrum of DMPA

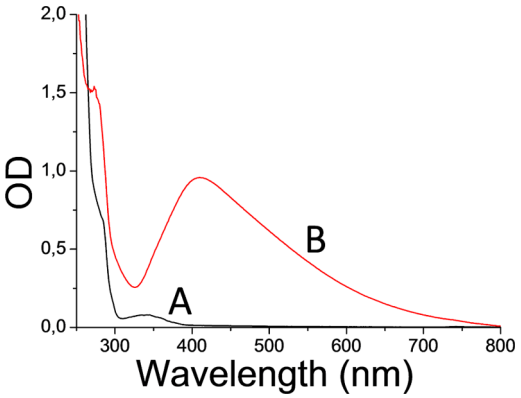

Figure 3. UV−visible spectrum of (A) DMPA/$AgSbF_6$ before irradiation and (B) DMPA/$AgSbF_6$ after 200 s of irradiation. Solvent = THF. Light intensity = 200 mW/cm^2.

mixed with silver salt ($AgSbF_6$) in oxygen-free THF under UV irradiation. The rapid increase (within ~200 s) of a large band with a maximum located at 410 nm can be safely assigned to the known silver surface plasmon resonance[63] of nanosized silver metal. The Ag NPs formation can be explained as

DOI: 10.1021/bm501755r
Biomacromolecules XXXX, XXX, XXX−XXX

resulting from the reduction of Ag^+ salt by benzoyl radical, generated from the photolysis of DMPA.[29]

Morphological analyses were carried out in order to confirm the presence of silver nanoparticles. SEM and FE-SEM micrographs, reported in Figure 4, show the presence of

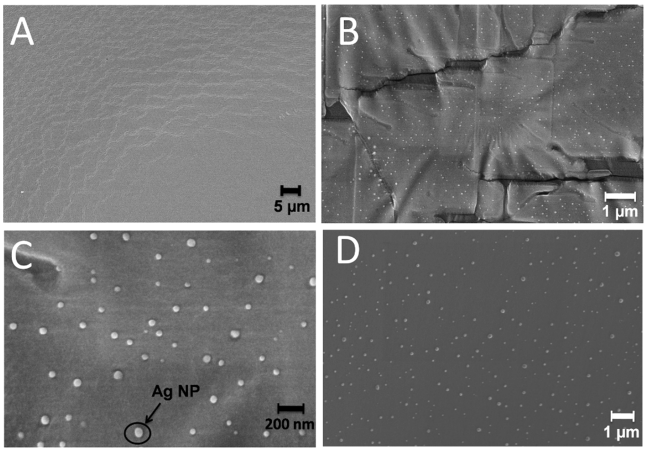

Figure 4. SEM images of the surface of the photoinduced films containing (A) DIALI/Trithiol/DMPA and (B, C) DIALI/Trithiol/DMPA/$AgSbF_6$. (D) FE-SEM image of the cross section of the photoinduced films containing Ag nanoparticles.

dispersed and distributed spherical silver NPs at the surface (and inside) of the polymer film with a diameter ranging from 30 to 150 nm (Figure 4B and C). It is also interesting to observe that the metal nanoparticles are homogeneously distributed within the thiol−ene-generated network as shown by the FE-SEM image of the cross section of the photoinduced film containing Ag nanoparticles (Figure 4D). Moreover, the transparency of the DIALI-derived films containing Ag NPs indicates that the Ag NPs are homogeneously dispersed inside the polymer films (Figure S2, Supporting Information). The morphological surfaces of both films are similar regardless of whether silver NPs are used. Cracks observed at the surface of both films are due to the high energy of the SEM electron beam used. The high local temperature of the focalized electron beam modifies the surface morphology of both films as they have a viscoelastic behavior (see the DMTA test results) at ambient temperature.

XPS measurements were performed to characterize the surface of the photoinduced biomaterials with or without silver NPs (Figure 5). As shown in Figure 5B, the XPS survey scan spectrum indicates the composition and structure of silver-containing DIALI. The carbon, sulfur, oxygen, and silver elements are found from the survey spectra of the nanocomposite materials, which are consistent with the chemical components of the silver photoinduced biomaterials. We focused our attention on the Ag 3d core level emission from the thiol−ene-generated hybrid coating containing 2 wt % silver salt. The XPS spectrum reported in Figure 5B exhibits a typical Ag 3d doublet at a binding energy of 373 eV with a doublet splitting of 6 eV. The position of these two peaks (373 eV for Ag $3d_{3/2}$ and 367 eV for Ag $3d_{5/2}$) clearly indicates that silver is present as metal (Ag^0).[64,65]

Mechanical analyses of the isosorbide-derived films (with and without Ag NPs) have been also studied, and results are displayed in Figure 6. Viscoelastic characterization was performed, in a very large temperature interval, by dynamic-

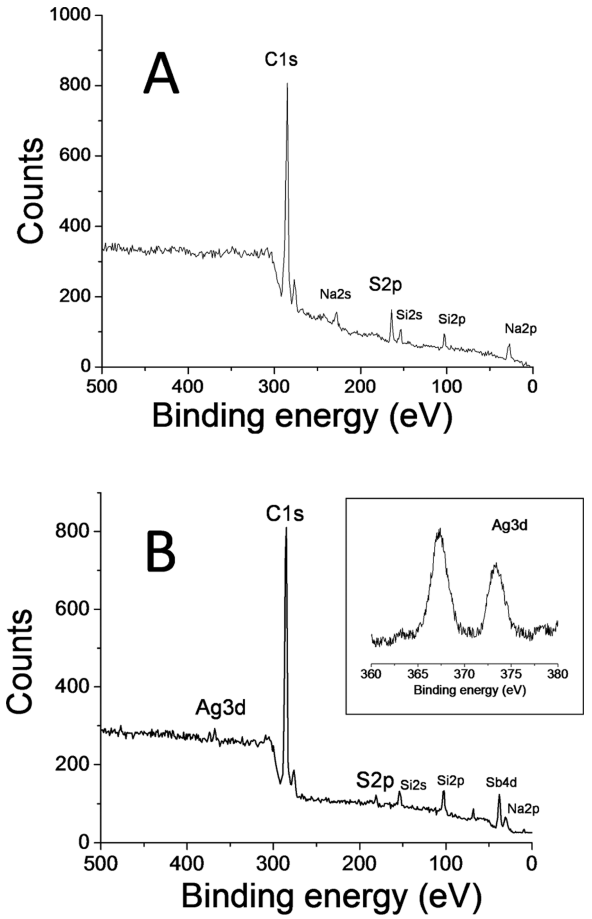

Figure 5. XPS survey spectrum of the photoinduced coatings containing (A) DIALI/Trithiol/DMPA and (B) DIALI/Trithiol/DMPA/$AgSbF_6$. Inset: XPS spectra from the Ag 3d core levels.

mechanical thermal analysis (DMTA, Figure 6A), which allows the evaluation of the elastic (E' = storage modulus) and viscous (E'' = loss modulus) components of the viscoelastic modulus and the damping factor, tan δ (E''/E'), of the materials. The maximum of tan δ peak is attributed to the glass transition temperature (T_g) of the cross-linked material.

For the thiol−ene photocured system in the absence of silver NPs, the T_g is evaluated at −10 °C (Figure 6A, curve 1) whereas it reaches −2 °C with the addition of silver NPs (Figure 6A, curve 2). DSC experiments (not shown here) following the same trend as T_g were evaluated at −3 and 2 °C for films without Ag NPs and with Ag NPs, respectively. The slight increase of T_g is likely due to the interaction between the thiol−ene matrix and the metal NPs, which hinders the mobility of the polymeric chains, thus resulting in an increase of minor stiffness along with a decrease of the free-volume due to the presence of the metal NPs. The slight increase of T_g values does not affect significantly the viscoelastic behavior of the UV-cured film which maintains its rubbery state at room temperature. These results are in accordance with literature investigation in which, for example, Sangermano and co-workers[38] described the same phenomenon with allylpentaerythritol polymer matrix containing Ag NPs. Furthermore, the stress−strain test (Figure 6B) shows that the presence of Ag NPs induced an increase of modulus with an increasing slope of the curve observed for the filled material. The modulus

DOI: 10.1021/bm501755r
Biomacromolecules XXXX, XXX, XXX−XXX

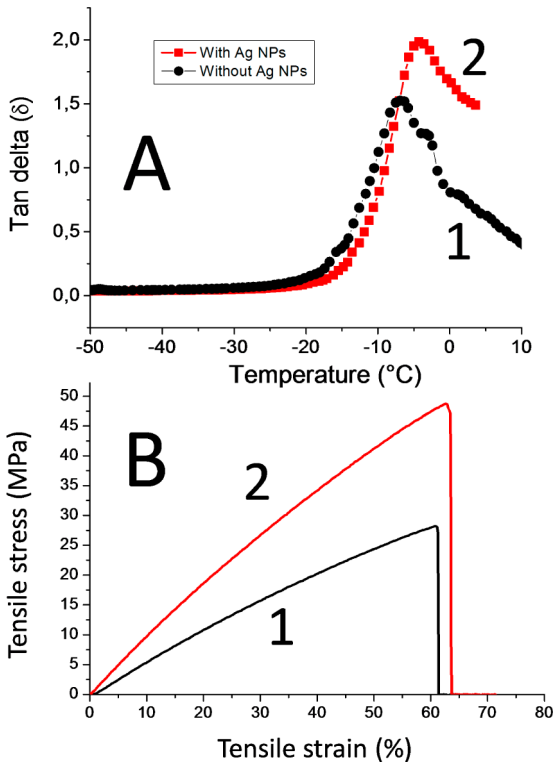

Figure 6. Mechanical analyses of the isosorbide-derived films with and without Ag NPs. (A) DMTA spectra of the photoinduced films containing (1) DIALI/Trithiol/DMPA and (2) DIALI/Trithiol/DMPA/$AgSbF_6$. (B) Tensile tests for (1) DIALI/Trithiol/DMPA films and (2) DIALI/Trithiol/DMPA/$AgSbF_6$ films.

increases in accordance with the higher stiffness attributed to the presence of the in situ generated Ag NPs.

The thermal stability of the photoinduced DIALI films (with and without Ag NPs) was studied by thermal gravimetric analysis (TGA) under argon atmosphere. The results are displayed in Figure 7. It can be observed that the two hybrid

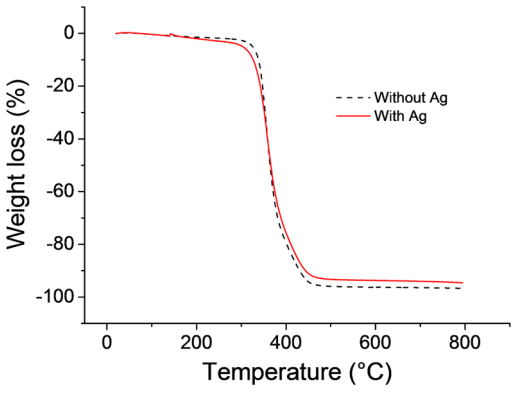

Figure 7. TGA thermograms of the photoinduced films containing (dashed line) DIALI/Trithiol/DMPA and (solid line) DIALI/Trithiol/DMPA/$AgSbF_6$.

films follow the same trend and yield thermal stability up to 320 °C. Both films reached 50% weight loss at 363 °C. These results are in accordance with some thiol−ene photopolymerizable systems which present thermal stability up to 300 °C described by Soucek et al.[66] and could be compared with the hybrid networks containing silsesquioxanes which have been developed by Versace et al.[67] according to the sol−gel chemistry process. The difference with the other investigations could be explained by the strength of the cross-linked network. The total mass loss observed at 600 °C for DIALI-derived film without Ag NPs is different from that of DIALI-derived film with Ag NPs: the difference is attributed to the introduction of the 2 wt % Ag NPs.

Photoinduced DIALI-Derived Materials Used as a Coating. The pencil hardness of the DIALI-derived coatings (with and without Ag NPs) is always above 7H, and no macroscopic scratch was evidenced on their surface. Moreover, no difference was observed on pencil hardness results with or without the use of Ag NPs. The high reticulation rate of the photopolymerized coatings hides the Ag NPs effect. In order to highlight more precisely the effect of the introduction of Ag NPs into coatings, further investigations, that is, nanoindentation tests, have been performed.

The loading and unloading curves during the nanoindentation tests are close to being superimposed, showing that both DIALI-derived coatings (with and without Ag NPs) have at room temperature a quasi-elastic behavior. This is attributed to the rubberlike state predicted by the low glass transition temperature of the two coatings (−10 and −2 °C). The elastic modulus E of the DIALI-derived coating without Ag NPs is found to be independent of the indentation depth and was evaluated at (9 ± 1) MPa. This value is in the range[68] (1−19 MPa) of the common elastomeric materials, that is, styrene−butadiene, isobutylene−isoprene, acrylonitrile−butadiene, poly(2-chloro-1,3-butadiene), and ethylene−propylene rubbers. For the sample containing Ag NPs, the value of the elastic modulus at the extreme surface is similar to the one described without Ag NPs, but increases with an increasing indentation depth, probably due to a stiffening effect of the Ag NPs.

Concerning the scratch resistance test (Figure 8), an increasing load leads to an increasing tensile stress at the contact, until it reaches the tensile strength resulting in the appearance of brittle fractures. These fractures release stress and leads to a decrease of the lateral force. The first peak on the scratch curves indicates the beginning of the fracture which afterward continuously developed along with the scratching

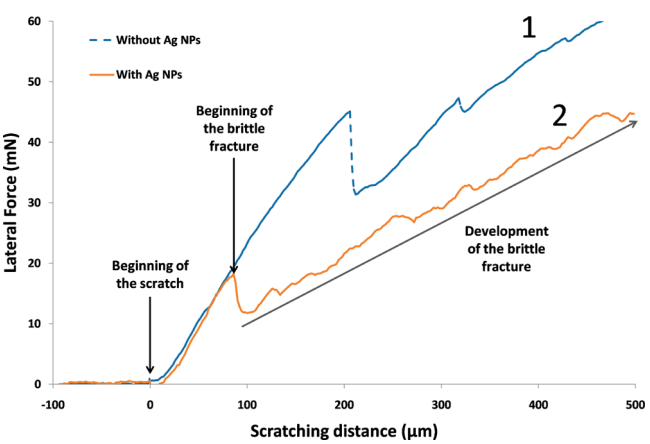

Figure 8. Friction force as a function of the scratching distance. Scratch resistance tests on isosorbide-derived coatings (1) without Ag NPs and (2) with Ag NPs. The load linearly increases from 0.1 to 200 mN between scratching distances from 0 to 500 μm. Thickness of the coatings deposited on glass substrate = 200 μm.

DOI: 10.1021/bm501755r
Biomacromolecules XXXX, XXX, XXX−XXX

distance. According to Hamilton,[69] the tensile strength could be computed and was estimated at (38 ± 6) MPa for both samples: this value is in the higher range of common elastomers[68] (1.2−30 MPa).

The presence of Ag NPs embedded in the coatings decreases the scratch resistance of the sample as the lateral force appears well lower than the one of coating without Ag NPs. Optical images of the scratched surfaces do not show any plastic deformation but brittle cracks (Figure 9). As expected from

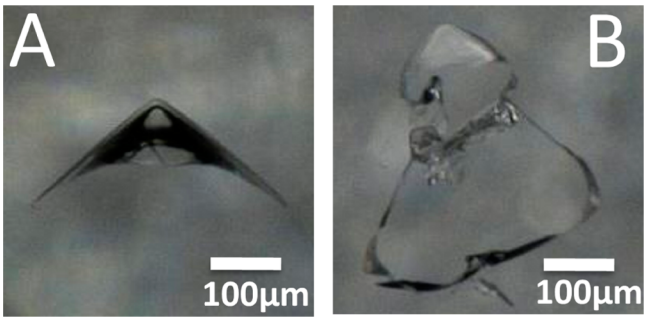

Figure 9. Brittle cracks for the two coatings without Ag NPs (A) and with Ag NPs (B).

DMTA tests and nanoindentation experiments, the coatings with and without Ag NPs have a rubberlike behavior and are not able of ductile deformation. The brittle fracture of the DIALI-derived coating containing Ag NPs is erratic and not reproducible, thus describing a heterogeneous material, whereas the fracture of the DIALI-derived coating without Ag NPs is symmetric and reproducible, which corresponds to a homogeneous material (Figure 9). Nevertheless, no delamination of both coatings is observed, showing a good adhesion to the glass substrate in comparison with the coating cohesion.

The mechanical properties of the two materials could be changed, according to the polymer specifications linked to its uses (coating, bulk material, etc.). The present coatings have a rubberlike behavior at room temperature which is interesting when a good adhesion to another surface is needed.[70] Tensile tests have shown that they can undergo elastic strain superior to 60% before fracture happens (Figure 6). They are thus adapted to coat compliant substrates as elastomers used in the fabrication of catheters (silicons, polyurethane, etc.) or textiles which are brought to undergo important strains during their use. We can thus intend to use these coatings for catheters with the aim of decreasing the risk of biofilm formation and reducing allergic intolerance.

This kind of coating could also be used on rigid substrates. Their elastomeric states increase their adhesive properties.[71] It is thus interesting to use them for hand-care utensils like pliers, for example. While the mechanical properties of elastomers do not confer them a good abrasive resistance, the isosorbide-derived coatings are more indented to be used for single-use utensils. Anyway, the advantage of impregnation of medical devices with Ag NPs is the protection of the inner and the outer surfaces of devices. But in order to increase the abrasion resistance of the isosorbide-derived coatings to stiffer substrates (as for example coating of hospital furniture), it is thus necessary to copolymerize isosorbide-derived monomers with other monomers containing benzyl groups or use multifunctional cross-linkers such as tetrathiol derivatives to increase the glass transition temperature beyond 40 °C. The resistance of the coating to wear could be improved by the addition of silica balls[72] or by using hybrid silica materials with photopolymerizable functions.[73]

Finally, the adhesion of the isosorbide-based coatings on polymeric substrates could be enhanced by introducing thiol or allylic double bonds on the surface of the polymer which has to be modified, thus leading to an increase of the strength chemical bonding between the isosorbide-derived coatings and the polymeric substrates.

Antibacterial Properties. The antimicrobial properties of silver nanoparticles into polymeric matrix demonstrated their effectiveness against bacteria adhesion on materials surface. Therefore, the ability of the silver nanoparticles embedded in the surface or released from the surface of the isosorbide-derived films to inhibit the bacterial adhesion was evaluated with Gram-positive *S. aureus* and Gram-negative *E. coli*.

Table 2 shows the results of the antibacterial tests performed on the photoinduced films with and without Ag NPs. The standard coating without Ag NPs does not exhibit antibacterial property, along with coatings containing 0.5 wt % Ag NPs, which do not significantly inhibit ($P > 0.05$) the *S. aureus* and *E. coli* adherence. In contrast, the introduction of Ag NPs into the DIALI-based material led to a drastic inhibition of the bacterial adhesion. Indeed, the DIALI/Ag material presented an average decrease of 91% and 84% of the adhered *S. aureus* and *E. coli*, respectively, in comparison with the DIALI material (without Ag NPs) used as a reference.

By increasing the incubation time (from 1 to 6 h) between the isosorbide-derived films containing Ag NPs and the different bacteria strains, an average decrease of 98% of the adhered *S. aureus* and *E. coli* was observed after 6 h. The remaining bacteria correspond to the live bacteria cells which can generate colonies according to the counting method used for evaluating the antiadherence properties of the films. In addition to these antibacterial results, the amount of silver NPs released from the polymer matrix was calculated using the inductively coupled plasma method. This is indispensable in the context of medical device safety. As shown in Figure 10, the amount of released silver nanoparticles moderately increased with the increase of incubation times, and it reached 0.21 ppm over the period of 16 days. Similar results were described by Kang et al.[74] with a PHBHV/Ag (1 wt %) electrospun nanofibrous scaffold, in which the concentration of silver NPs

Table 2. Comparison of the Antiadherence Property against *S. aureus* and *E. coli* of the Photoinduced Films with and without Ag NPs after Different Incubation Times[a]

	standard (without Ag NPs)	treatment (with 2 wt % Ag NPs)	
	1 h	1 h	6 h
CFU *S. aureus*	(1 ± 0.3) × 10^6	(0.09 ± 0.05) × 10^6	(0.03 ± 0.01) × 10^6
CFU *E. coli*	(5.1 ± 1.7) × 10^6	(0.9 ± 0.1) × 10^6	(0.1 ± 0.04) × 10^6

[a]Data are shown as means plus standard deviation, $n = 10$. Mean values are significantly different ($P < 0.05$).

DOI: 10.1021/bm501755r
Biomacromolecules XXXX, XXX, XXX−XXX

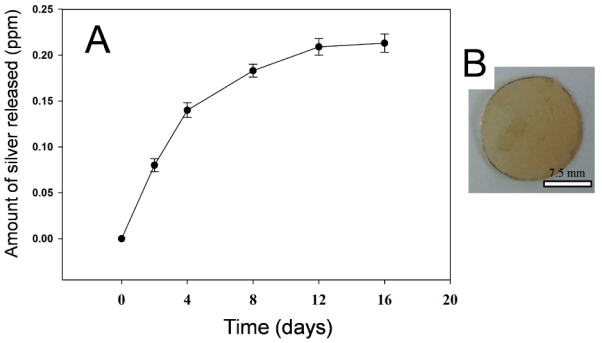

Figure 10. Release of Ag NPs from the isosorbide-derived films. (A) Amount of silver nanoparticles released from the DIALI containing Ag NPs films as a function of the immersion time and (B) optical image of the DIALI-derived film containing Ag NPs.

released was evaluated at 0.237 ppm after only 8 days with an efficient antibacterial effect. In our investigation, the rate of release is lower than that described by Kang et al.,[74] and we could expect a long-term antibacterial effect.

Despite the slow release of silver NPs through the isosorbide-derived films according to the ICP experiments (Figure 10), the decrease of the number of *S. aureus* and *E. coli* CFUs after 6 h of incubation (Table 2) demonstrates that Ag NPs, and particularly the Ag NPs present at the surface of the films, are the only species responsible for the antiadherence and antibacterial property of the Ag containing materials. According to the literature studies, bacterial inhibition of Ag NPs is caused by the combination of bacteriostatic and bacteriocidal effects, which is governed by two different mechanisms of action:[75,76] first, Ag NPs attach to the surface of the cell membrane and disturb its main functionalities, such as the permeability and the respiration process. The inhibition of the bacterial cell wall synthesis in *S. aureus* bacteria was reported by Song et al.[77] In the case of *E. coli*, Ag NPs lead to the inhibition of phosphate uptake and cause the loss of phosphate, and some amino acids like proline or glutamine from *E. coli* cells.[78] The interaction between these NPs and the bacterial cells are favored because of the large surface area of the synthesized Ag NPs (located at the surface of the films) which could stay in contact with the bacteria.[79] Second, the Ag NPs which may diffuse through the polymeric film are able to penetrate the bacteria by interacting with sulfur- and phosphorus-containing compounds (such as DNA) constituting the cell membrane.[80] For example, Raffi and co-workers[81] reported transmission electron microscopy images of the Ag NPs diffusion in the membrane and inside the bacteria. In addition, they demonstrated the inactivation of their enzymes by Ag NPs, thus leading to the formation of hydrogen peroxide and causing bacterial cell death.[81] Considering these effects, the detachment of the Ag NPs from the surface of the isosorbide-derived films is not necessary to cause antibacterial effect especially when bacteriostatic effect is mainly caused by the attached Ag NPs.

These results clearly indicated that the incorporation of silver nanoparticles on the photoinduced material is a powerful method for substantially enhancing the antibacterial properties, and thus preventing the adherence of bacteria on the film surface.

Cytocompatibility. In this study, NIH 3T3 fibroblast cells were used to evaluate the cytotoxicity of silver NPs. Figures 11 and 12 show the NIH 3T3 fibroblasts adhesion on the surface of the composite films (with and without Ag NPs) after 1 and 3 days, respectively. The surface morphology of the samples was observed by FE-SEM. Figure 11A and B represents the control sample, and Figure 11C and D represents the composite film containing Ag NPs. From the SEM images (Figure 11), it was observed that fibroblast cells had adhered to both DIALI-derived films regardless of the presence of Ag NPs in the composite sample after 1 day and exhibited a round-shape morphology. After 3 days, Figure 12 illustrates the change of cell morphology, that is, from a spherical shape to a flattened one for both DIALI-derived films. It is interesting to point out that the communication channels, which are indispensable for the cell differentiation or other cell information, were already noticeable for both DIALI-derived films with and without Ag NPs. The production of these communication channels also named slender cytoplasmic projections allowed to improve the focal cell adhesion on the surface of the DIALI-derived films. Figure 13 shows that the proliferation of NIH 3T3 fibroblastic cells cultured for 1 and 3 days on the surface of the photoinduced films. Cell proliferation on the DIALI-derived films without Ag NPs appears to be the same as the one on silver-containing DIALI films within the standard deviation and the number of cells increases by a 1.8 factor between 1 and 3 days. Viability of the cells after 3 days on both the DIALI-derived films (with and without Ag NPs) was observed using live/dead assays (Figure 14). The fluorescence color of the cells cultured on the DIALI-derived films (without Ag NPs) was

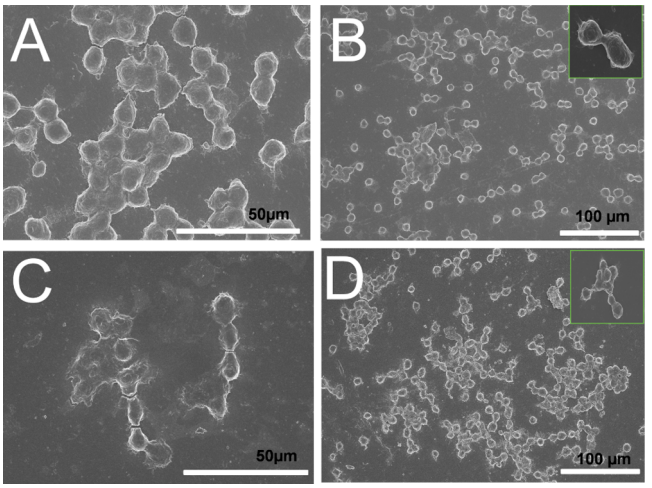

Figure 11. FE-SEM images of the fibroblast cells (NIH 3T3) adhesion after 1 day on the DIALI-derived material without silver NPs (A and B) and composite material with silver NPs (C and D).

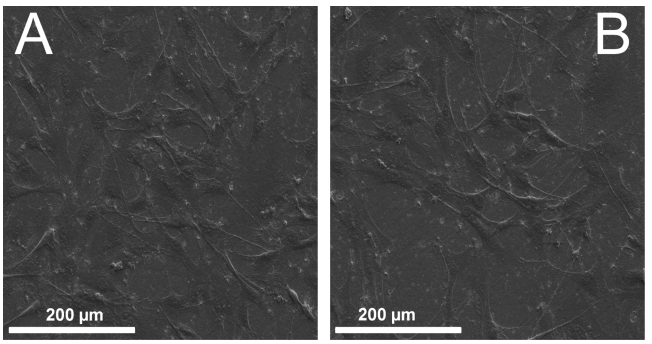

Figure 12. FE-SEM images of the fibroblast cells (NIH 3T3) adhesion after 3 days on the DIALI-derived material without silver NPs (A) and composite material with silver NPs (B).

DOI: 10.1021/bm501755r
Biomacromolecules XXXX, XXX, XXX−XXX

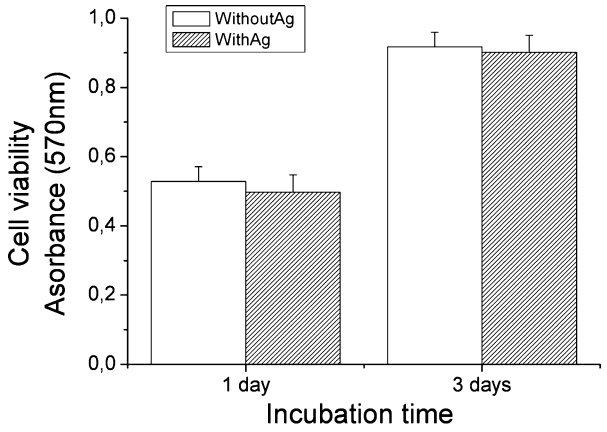

Figure 13. Proliferation of NIH 3T3 cells cultured for 3 days using MTT assay. Data expressed as mean ± standard deviation (n = 6) for the specific absorbance.

totally green, thus indicating a good viability of the cells (Figure 14A–C). On the contrary, a few dead cells, which are characterized by red fluorescence with the introduction of propidium iodide, have been observed on the surface of DIALI-derived films with Ag NPs (Figure 14D, see the white arrows). It is also interesting to notice that no dead cells were observed on the other part of the surface of the DIALI-derived films with Ag NPs (Figure 14E and F). As demonstrated in this investigation, low cell cytotoxicity and high antibacterial property against *S. aureus* and *E. coli* are observed for DIALI-derived films containing silver NPs with 2 wt %.

CONCLUSIONS

Silver-containing DIALI materials with antibacterial property were engineered and then characterized by DMTA, FE-SEM, and XPS analysis. The results demonstrated that the photo-induced Ag NPs, which are in situ generated upon light irradiation according to a fast photoreduction process, were randomly and homogeneously distributed on the surface and within the composite films. The resulting DIALI material including silver nanoparticles led to a reduction by 98% of the adherence of *S. aureus* and *E. coli* after 6 h of incubation without significantly affecting the adhesion and proliferation of NIH 3T3 fibroblastic cells. Finally, these isosorbide-derived materials could be also used as coatings according to their rubberlike state and are thus adapted to coat compliant substrates such as elastomers used in the fabrication of catheters (silicons, polyurethane), textiles, or hand-care utensils like pliers.

ASSOCIATED CONTENT

Supporting Information

^{1}H and ^{13}C NMR spectra of DIALI (Figure S1); optical images of the DIALI-derived films (Figure S2) and DIALI-derived coatings with and without Ag NPs (Figure S3); specimen for mechanical test performance (Figure S4) and optical images of the circular DIALI-derived films used for cell adhesion and proliferation (Figure S5). This material is available free of charge via the Internet at http://pubs.acs.org.

AUTHOR INFORMATION

Corresponding Author

*E-mail: versace@icmpe.cnrs.fr. Telephone: +33 149781228.

Notes

The authors declare no competing financial interest.

ACKNOWLEDGMENTS

We would like to thank the CNRS institute and UPEC for financial support.

REFERENCES

(1) Munoz-Bonilla, A.; Fernandez-Garcia, M. *Prog. Polym. Sci.* **2012**, *37*, 281–339.
(2) Lim, K. S.; Oh, K. W.; Kim, S. H. *Polym. Int.* **2012**, *61*, 1519–1524.
(3) Perni, S.; Piccirillo, C.; Pratten, J.; Prokopovich, P.; Chrzanowski, W.; Parkin, I. P.; Wilson, M. *Biomaterials* **2009**, *30*, 89–93.
(4) Decraene, V.; Pratten, J.; Wilson, M. *Appl. Environ. Microbiol.* **2006**, *72*, 4436–4439.

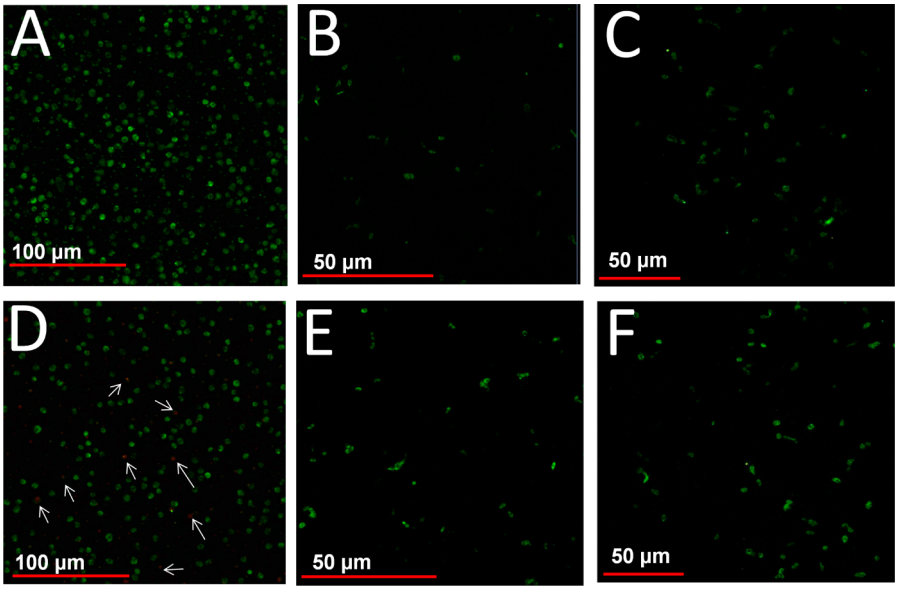

Figure 14. Live/dead assays: fluorescence microscopy images of NIH 3T3 cells cultured for 3 days on the DIALI-derived films without Ag NPs (A–C) and composite material with Ag NPs (D–F). White arrows display the dead cells.

DOI: 10.1021/bm501755r
Biomacromolecules XXXX, XXX, XXX–XXX

(5) Matsunaga, T.; Tomoda, R.; Nakajima, T.; Nakamura, N.; Komine, T. *Appl. Environ. Microbiol.* **1988**, *54*, 1330−1333.
(6) Ruckh, T. T.; Oldinski, R. A.; Carroll, D. A.; Mikhova, K.; Bryers, J. D.; Popat, K. C. *J. Mater. Sci.: Mater. Med.* **2012**, *23*, 1411−1420.
(7) Lu, J.; Hill, M. A.; Hood, M.; Greeson, J. D. F.; Horton, J. R.; Orndorff, P. E.; Herndon, A. S.; Tonelli, A. E. *J. Appl. Polym. Sci.* **2001**, *82*, 300−309.
(8) Chung, D.; Papadakis, S. E.; Yam, K. L. *Int. J. Food Sci. Technol.* **2003**, *38*, 165−169.
(9) Knetsch, M. L. W.; Koole, L. H. *Polymers* **2011**, *3*, 340−366.
(10) Amna, T.; Hassan, M. S.; Barakat, N. A. M.; Pandeya, D. R.; Hong, S. T.; Khil, M.-S.; Kim, H. Y. *Appl. Microbiol. Biotechnol.* **2012**, *93*, 743−751.
(11) Tang, Z.; Kotov, N. A.; Magonov, S.; Ozturk, B. *Nat. Mater.* **2003**, *2*, 413−418.
(12) Pant, H. R.; Pandeya, D. R.; Nam, K. T.; Baek, W.-I.; Hong, S. T.; Kim, H. Y. *J. Hazard. Mater.* **2011**, *189*, 465−471.
(13) Kim, S. H.; Kwak, S.-Y.; Sohn, B.-H.; Park, T. H. *J. Membr. Sci.* **2003**, *211*, 157−165.
(14) Elzatahry, A. A.; Al-Enizi, A. M.; Elsayed, E. A.; Butorac, R. R.; Al-Deyab, S. S.; Wadaan, M. A.; Cowley, A. H. *Int. J. Nanomed.* **2012**, *7*, 2829−2832.
(15) Wu, J.; Hou, S.; Ren, D.; Mather, P. T. *Biomacromolecules* **2009**, *10*, 2686−2693.
(16) Jensen, E. L.; Rungby, J.; Hansen, J. C.; Schmidt, E.; Pedersen, B.; Dahl, R. *Hum. Toxicol.* **1988**, *7*, 535−540.
(17) Cohen, M. S.; Stern, J. M.; Vanni, A. J.; Kelley, R. S.; Baumgart, E.; Field, D.; Libertino, J. A.; Summerhayes, I. C. *Surg. Infect.* **2007**, *8*, 397−404.
(18) Chaloupka, K.; Malam, Y.; Seifalian, A. M. *Trends Biotechnol.* **2010**, *28*, 580−588.
(19) Liu, X.; Lin, T.; Fang, J.; Yao, G.; Zhao, H.; Dodson, M.; Wang, X. *J. Biomed. Mater. Res., Part A* **2010**, *94*, 499−508.
(20) Chaudhry, Q.; Scotter, M.; Blackburn, J.; Ross, B.; Boxall, A.; Castle, L.; Aitken, R.; Watkins, R. *Food Addit. Contam., Part A* **2008**, *25*, 241−258.
(21) Wu, W. T.; Wang, Y.; Shi, L.; Zhu, Q.; Pang, W.; Xu, G.; Lu, F. *Nanotechnology* **2005**, *16*, 3017−3022.
(22) Pastoriza-Santos, I.; Liz-Marzan, L. M. *Langmuir* **1999**, *15*, 948−951.
(23) Yu, Y. Y.; Chang, S. S.; Lee, C. L.; Wang, C. R. C. *J. Phys. Chem. B* **1997**, *101*, 6661−6664.
(24) Reetz, M. T.; Helbig, W. *J. Am. Chem. Soc.* **1994**, *116*, 7401−7402.
(25) Scaiano, J. C.; Aliaga, C.; Maguire, S.; Wang, D. *J. Phys. Chem. B* **2006**, *110*, 12856−12859.
(26) Marin, M. L.; McGilvray, K. L.; Scaiano, J. C. *J. Am. Chem. Soc.* **2008**, *130*, 16572−16584.
(27) Scaiano, J. C.; Stamplecoskie, K. G.; Hallett-Tapley, G.-L. *Chem. Commun.* **2012**, *48*, 4798−4808.
(28) Stamplecoskie, K. G.; Scaiano, J. C. *Photochem. Photobiol.* **2012**, *88*, 762−768.
(29) Scaiano, J. C.; Billone, P.; Gonzales, C. M.; Maretti, L.; Marin, M. L.; McGilvray, K. L.; Yuan, N. *Pure Appl. Chem.* **2009**, *81*, 635−647.
(30) Versace, D. L.; Bastida, J. C.; Lorenzini, C.; Cachet-Vivier, C.; Renard, E.; Langlois, V.; Malval, J.-P.; Fouassier, J.-P.; Lalevée, J. *Macromolecules* **2013**, *46*, 8808−8815.
(31) Versace, D. L.; Ramier, J.; Grande, D.; Andaloussi, S. A.; Dubot, P.; Hobeika, N.; Malval, J.-P.; Lalevee, J.; Renard, E.; Langlois, V. *Adv. Healthcare Mater.* **2013**, *2*, 1008−1018.
(32) Fouassier, J. P.; Rabek, J. F. *Radiation curing in polymer science and technology*; Fouassier, J. P., Rabek, J. F., Eds.; Elsevier Applied Science: London, New York, 1993; Vol. *1*.
(33) Fouassier, J.-P.; Lalevée, J. *Photoinitiators for Polymer Synthesis: Scope, Reactivity, and Efficiency*; John Wiley & Sons: Weinheim, Germany, 2013.
(34) Yagci, Y.; Sangermano, M.; Rizza, G. *Polymer* **2008**, *49*, 5195−5198.
(35) Yagci, Y.; Sangermano, M.; Rizza, G. *Chem. Commun.* **2008**, 2771−2773.
(36) Yagci, Y.; Sangermano, M.; Rizza, G. *Macromolecules* **2008**, *41*, 7268−7270.
(37) Yagci, Y.; Jockusch, S.; Turro, N. J. *Macromolecules* **2010**, *43*, 6245−6260.
(38) Colucci, G.; Celasco, E.; Mollea, C.; Bosco, F.; Conzatti, L.; Sangermano, M. *Macromol. Mater. Eng.* **2011**, *296*, 921−928.
(39) Gandini, A. *Macromolecules* **2008**, *41*, 9491−9504.
(40) Coates, G. W.; Hillmyer, M. A. *Macromolecules* **2009**, *42*, 7987−7989.
(41) Belgacem, M. N.; Gandini, A. *Monomers, Polymers and Composites from Renewable Resources*, 1st ed.; Belgacem, M. N., Gandini, A., Eds.; Elsevier Academic Press: Amsterdam, 2008.
(42) Galbis, J. A.; Garcia-Martin, M. G. In *Monomers, Polymers and Composites from Renewable Resources*, 1st ed.; Belgacem, M. N., Gandini, A., Eds.; Elsevier Academic Press: Amsterdam, 2008; p 89.
(43) Feng, X.; East, A. J.; Hammond, W. B.; Zhang, Y.; Jaffe, M. *Polym. Adv. Technol.* **2011**, *22*, 139−150.
(44) Fenouillot, F.; Rousseau, A.; Colomines, G.; Saint-Loup, R.; Pascault, J. P. *Prog. Polym. Sci.* **2010**, *35*, 578−622.
(45) Rose, M.; Palkovits, R. *ChemSusChem* **2012**, *5*, 167−176.
(46) Chrysanthos, M.; Galy, J.; Pascault, J. P. *Polymer* **2011**, *52*, 3611−3620.
(47) Lukaszczyk, J.; Janicki, B.; Kaczmarek, M. *Eur. Polym. J.* **2011**, *47*, 1601−1606.
(48) Jasinska, L.; Konig, C. E. *J. Polym. Sci., Part A: Polym. Chem.* **2010**, *48*, 2885−2895.
(49) Noordover, B.; Haveman, D.; Duchateau, R.; Benthem, R. V.; Konig, C. E. *J. Appl. Polym. Sci.* **2011**, *121*, 1450−1463.
(50) Kricheldorf, H. R.; Sun, S.-J.; Sapich, B.; Stumpe, J. *Macromol. Chem. Phys.* **1997**, *198*, 2197−2210.
(51) Ortiz, R. A.; Martinez, A.; Valdez, A. E. G. *J. Biobased Mater. Bio.* **2012**, *6*, 36−41.
(52) Lukaszczyk, J.; Janicki, B.; Frick, A. *J. Mater. Sci-Mater. M.* **2012**, *23*, 1149−1155.
(53) Haider, A.; Gupta, K. C.; Kang, I.-K. *Biomed. Res. Int.* **2014**, DOI: 10.1155/2014/308306.
(54) Kim, H. M.; Chae, W. P.; Chang, K. W.; Chun, S.; Kim, S.; Jeong, Y.; Kang, I.-K. *J. Biomed. Mater. Res., Part B* **2010**, *94B*, 380−387.
(55) Shin, Y.-S.; Borah, J. S.; Haider, A.; Kim, S.; Huh, M.-W.; Kang, I.-K. *J. Nanomater.* **2013**, DOI: 10.1155/2013/404210.
(56) Hoyle, C. E.; Bowman, C. N. *Angew. Chem., Int. Ed.* **2010**, *49*, 1540−1573.
(57) Criqui, A.; Lalevée, J.; Allonas, X.; Fouassier, J.-P. *Macromol. Chem. Phys.* **2008**, *209*, 2223−2231.
(58) Pan, X.; Lacôte, E.; Lalevée, J.; Curran, D. P. *J. Am. Chem. Soc.* **2012**, *134*, 5669−5674.
(59) Sangermano, M.; Yagci, Y.; Rizza, G. *Macromolecules* **2007**, *40*, 8827−8829.
(60) Caro, C.; López-Cartes, C.; Zaderenko, P.; Mejías, J. A. *J. Raman Spectrosc.* **2008**, *39*, 1162−1169.
(61) Ostuni, E.; Yan, L.; Whitesides, G. M. *Colloids Surf., B* **1999**, *15*, 3−30.
(62) Weber, M.; Khudyakov, I. V.; Turro, N. J. *J. Phys. Chem. A* **2001**, *106*, 1938−1945.
(63) Maillard, M.; Huang, P.; Brus, L. *Nano Lett.* **2003**, *3*, 1611−1615.
(64) Thomas, S.; Nair, S. K.; Jamal, E. M. A.; Al-Harthi, S. H.; Varma, M. R.; Anantharaman, M. R. *Nanotechnology* **2008**, *18*, 075710.
(65) Barrie, A.; Christensen, N. E. *Phys. Rev. B* **1976**, *14*, 2442−2447.
(66) Ortiz, R. A.; Urbina, B. A. P.; Santos, R. G.; Duarte, L. B.; Valdez, A. E. G.; Soucek, M. D. *Macromol. Mater. Eng.* **2008**, *293*, 731−739.
(67) Lorenzini, C.; Versace, D. L.; Gaillet, C.; Lorthioir, C.; Boileau, S.; Renard, E.; Langlois, V. *Polymer* **2014**, *55*, 4432−4440.
(68) Mark, J. E. *Physical properties of polymers handbook*; American Institute of Physics: Woodbury, NY, 1996.

DOI: 10.1021/bm501755r
Biomacromolecules XXXX, XXX, XXX−XXX

(69) Hamilton, G. M. *Proc. - Inst. Mech. Eng.* **1983**, *197C*, 53−59.
(70) Barquins, M. *Wear* **1992**, *158*, 87−117.
(71) Maugis, D. *J. Colloid Interface Sci.* **1992**, *150*, 243−269.
(72) Vu, C.; Laferté, O.; Eranian, A. *Eur. Coat. J.* **2002**, *1*−*2*, 64−70.
(73) Schottner, G. *Chem. Mater.* **2001**, *13*, 3422−3435.
(74) Xing, Z.-C.; Chae, W.-P.; Baek, J.-Y.; Choi, M.-J.; Jung, Y.; Kang, I.-K. *Biomacromolecules* **2010**, *11*, 1248−1253.
(75) Feng, Q. L.; Wu, J.; Chen, G. Q.; Cui, F. Z.; Kim, T. N.; Kim, J. O. *J. Biomed. Mater. Res.* **2000**, *52*, 662−668.
(76) Rai, M.; Yadav, A.; Gade, A. *Biotechnol. Adv.* **2009**, *27*, 76−83.
(77) Song, H. Y.; Ko, K. K.; Oh, I. H.; Lee, B. T. *Eur. Cells Mater.* **2006**, *11*, 58−59.
(78) Yamanaka, M.; Hara, K.; Kudo, J. *Appl. Environ. Microb.* **2005**, *71*, 7589−7593.
(79) Pal, S.; Tak, Y. K.; Song, J. M. *Appl. Environ. Microb.* **2007**, *27*, 1712−1720.
(80) Gibbins, B.; Warner, L. *Med. Device Diagn. Ind. Mag.* **2005**, *1*, 1−2.
(81) Raffi, M.; Hussain, F.; Bhatti, T. M.; Akhter, J. I.; Hameed, A.; Hasan, M. M. *J. Mater. Sci. Technol.* **2008**, *24*, 192−196.

DOI: 10.1021/bm501755r
Biomacromolecules XXXX, XXX, XXX−XXX